



ORIGINAL ARTICLE

Copper based azo dye catalysts for phenoxazinone synthase mimicking efficiency: Structure characterization and bioactivity evaluation



Hoda A. El-Ghamry^{a,b,*}, Azah A. Alkurbi^{a,*}, Mona A. Alhasani^a,
Khadiga M. Takroni^a, Abdalla M. Khedr^b

^a Chemistry Department, Faculty of Applied Science, Umm Al-Qura University, Makkah, Saudi Arabia

^b Chemistry Department, Faculty of Science, Tanta University, Tanta, Egypt

Received 24 February 2023; accepted 10 April 2023

Available online 17 April 2023

KEYWORDS

Copper chelates;
Different anions;
Sulfonamides;
Biological efficiency;
Catalytic activity

Abstract The ligands, 4-(2-Hydroxy-naphthalen-1-ylazo)-N-thiazol-2-yl-benzenesulfonamide (**H₂TNBS**) and N-(3,4-Dimethyl-isoxazol-5-yl)-4-(2-hydroxy-naphthalen-1-ylazo)-benzenesulfonamide (**H₂INBS**), synthesized in the current investigation have been characterized and used for synthesizing divalent copper complexes by their reaction with a number of Cu(II) salts. Spectral and analytical methods have been applied for structures' investigation. Morphology of the synthesized compounds have been investigated using TEM technique which joint with the results of X-ray powder diffraction spectroscopy confirmed the precipitation of both ligands and their complexes in the nanometric scale. Formation of the synthesized complexes in 1:1 or 2:1 (M:L) ratio was asserted by analytical results. Ultraviolet–visible spectra and magnetic moment were used to demonstrate the geometry around the Cu centers to be 4 coordinated square planar. The compounds under interest have been screened against selected microorganisms including Gram-positive and Gram-negative bacteria, unicellular and multicellular fungus showing, in most compounds, enhancement of activity upon chelation. The cell lines **A-549** (human lung cancer cell line) and **Panc-1** (human pancreatic cancer cell line) have been chosen to check the antitumor efficiency of the synthesized compounds; Vinblastine was used as standard. Finally, the Cu(II) chelates were investigated toward mimicking the protein phenoxazinone synthase using *o*-aminophenol (OAP) as substrate and DMF is the solvent. The results presented extremely high activity for the chloro complex **4** and nitro complex **6**

* Corresponding authors at: Chemistry Department, Faculty of Applied Science, Umm Al-Qura University, Makkah, Saudi Arabia.
E-mail addresses: haelghamry@uqu.edu.sa (H.A. El-Ghamry), s44286910@st.uqu.edu.sa (A.A. Alkurbi).

Peer review under responsibility of King Saud University.



with TOF numbers from 390.48 and 467.01 h⁻¹, respectively. The least activity afforded by the acetato complexes **2** and **5**.

© 2023 The Author(s). Published by Elsevier B.V. on behalf of King Saud University. This is an open access article under the CC BY license (<http://creativecommons.org/licenses/by/4.0/>).

1. Introduction

Since the discovery of the antibacterial efficiency of the first obtained sulfonamide compound by Gerhard Domagk (Bentley, 2009), non-countable number of synthetic drugs based on the class of compounds known as sulfa drugs have been utilized (Gawrońska et al., 2022). In addition to the well-recognized antibacterial efficacy (Kamal et al., 2007) of such class of compounds, they also reported to have characteristics as anticancer (Scozzafava et al., 2003), diuretic (Supuran, 2008), hypoglycemic (Kumasaka et al., 2003), anti-inflammatory (Weber et al., 2004), and carbonic anhydrase inhibitory (Gokcen et al., 2016) characteristics. They are also capable of inhibiting the metabolic in folic acid and then limit the cell proliferation (Feng et al., 2022; Mizdal et al., 2018) as analogous to p-aminobenzoic acid and so sulfonamides are used to treat nocardiosis and acute urinary tract contagions trigger by a number of microorganisms such as *Escherichia coli*, and *Proteus mirabilis*. The biological significance of sulfonamides is largely concerned with their 4-aminophenyl sulfonamide core structure, that can endure alternative substituting groups at sulfonamide N, sulfanilamide's hydrogen bond or as an aromatic heterocyclic ring in another sulfa drugs (Gaffer, 2019). Among the various sulfonamide derivatives, sulfisoxazole and sulfathiazole were established. Sulfanilamide is the source used for the syntheses of sulfisoxazole; which is a well-known antibacterial drug (Uhlemann et al., 2018; Gladys et al., 2003). Sulfisoxazole, with a weak acidic character, has been applied to treat acute otitis, chronic otitis prevention, and acute urinary tract infections (Althagafi et al., 2019).

Additionally, alteration of the sulfonamides' structures can lead to motivation and expansion of their biological characteristics (Wan et al., 2021; Guo et al., 2019; Xu et al., 2020). Among the ways which are used to improve the sulfonamides' structures is their implementation for the synthesis of azo dyes.

For a variety of biological uses, azo dyestuffs have attracted great attention. They were categorized as xenobiotic substances with biodegradation resistant character. They were employed, among other things, as biological stains, textile and food colorants, and acid/base indicators. In the treatment with Prontosil, the first sulfonamide-based azo drug, that was used in defense against streptococcal infections in mice, the azo bond has been exploited in pharmaceuticals to shield medications from unfavorable responses (Khattab et al., 2016; Islam et al., 2010). Heterocyclic azo dyes have given a share to the evolution of the branch of coordination chemistry. Different transition metal elements in low oxidation states are normalized using heterocyclic azo dye derivatives. These substances stand out for their biological effectiveness, analytical uses and catalytic performance (Islam et al., 2010; Saad et al., 2019; Khan et al., 2022). Azo dyes are frequently utilized in many industries, including those of textiles, leather, plastics, paper, liquid crystal displays in addition to laser & inkjet printers (Benkhaya et al., 2020). Due to their value as models for biological systems, it has been discovered that sulfa containing medicines incorporating azo groups are of significant interest in the medical profession (Saad et al., 2017; Mohamed and Mabrouk, 2006; Awad et al., 2010). More interestingly, and due to the accessibility to a large number of potential donor atoms, the fascinating structural variety, the flexibility, and the tendency to ligation as neutral or in patterned form, sulfonamide and its azo analogues offer a wide range of uses as potential bonds with numerous metal ions (Islam et al., 2010; Saad et al., 2019; Khan et al., 2022).

What is appearing to be more interesting is the ability of sulfonamides and their azo derivatives to form complexes with numerous numbers of metal ions with promising biological activity. Thus, these

derivatives can be used to design and create novel drugs which exhibit, in most cases, enhanced activity when compared with the unbound compounds (Saad et al., 2019; Saad et al., 2017; Samper et al., 2017). So, the principles of selecting the metal ion as well as the coordination ligands are of a great importance.

Copper, as element number 3 to being the most common transition metal that exists in living system, is a crucial whit metal found in both plants and animals and enables the biological iron uptake. It is a part of many enzymes' structures (Lee et al., 2021). In addition to its relevance as a trace metal, copper plays a vital role in the biochemistry of humans as component in many externally administered substances while it can connect to albumin and alternative proteins in addition to its ability to bind to a number of ligands, where these complexes can interact with biomolecules, notably proteins and nucleic acids (Iakovidis et al., 2011). Copper-containing metalloenzymes in biological systems perform as dioxygen and substrate activators for a number of bio-functions, including the effectiveness of phenoxazinone synthase which is a naturally occurring enzyme found in the bacteria *Streptomyces* antibiotics and catalyzes the oxidative coupling of *o*-aminophenol (OAP) derivatives into phenoxazinone chromophore (Phz). In practice, the latter is used to treat tumor types such as Wilm's tumor and other types of tumors by inhibiting the synthesis of RNA from DNA through DNA intercalation (Sarkar et al., 2017). Therefore, the phenoxazinone synthase is one of the enzymes whose structure is frequently imitated. The fundamental prerequisite for a metal complex to demonstrate prospective phenoxazinone synthase-like efficacy is the existence of labile sites on the metal centers.

As a result of all the previous finding, the current study primarily focuses on preparation and structure investigation two newly designed azo ligands and six of their copper complexes by the reaction of these azo ligands which are named 4-(2-Hydroxy-naphthalen-1-ylazo)-N-thiazol-2-yl-benzenesulfonamide (**H₂TNBS**) and N-(3,4-Dimethyl-isoxazol-5-yl)-4-(2-hydroxy-naphthalen-1-ylazo)-benzenesulfonamide (**H₂INBS**) with three different copper salts. The structure and spectral characteristic of the produced compounds have been studied extensively. The produced complexes' antibacterial, anticancer, and phenoxazinone synthase-like activity towards oxidation of *o*-aminophenol (OAP) to 2-aminophenoxazine-3-one (APX) have been assigned and described.

2. Experimental

2.1. Chemicals and instruments

All of the reagents employed in this investigation, which are analytical grade and employed as they received, were provided by Sigma-Aldrich company. Details about the tools and methods used for structure assertion and implementation is provided in part S1 (supplementary file).

2.2. Preparation of **H₂TNBS** (**Z**) and **H₂INBS** (**G**) ligands

The current azo ligands named 4-(2-hydroxy-naphthalen-1-yl azo)-N-thiazol-2-yl-benzenesulfonamide (**H₂TNBS**) and N-(3,4-dimethyl-isoxazol-5-yl)-4-(2-hydroxy-naphthalen-1-ylazo)-benzenesulfonamide (**H₂INBS**) have been prepared in a similar way to literature method (Khedr et al., 2019; Khedr et al., 2022). In this method, 2.55 gm (0.01 mol) of sulfathiazole

and 2.67 gm (0.01 mol) of sulfafurazole were separately dissolved in 25 ml of distilled H₂O which acidified by the addition of 2.5 ml (12 M, 0.03 mol) of concentrated HCl. These solutions were then kept at temperature below zero before the addition of sodium nitrite (0.69 g and 0.01 mol) solution. The process of adding of sodium nitrite solution should be done very slowly to enable the formation and stabilization of diazonium chloride. These solutions were added in the last step to aqueous solutions containing 1.44 g of 2-naphthol (0.01 mol) and 0.4 g (0.01 mol) of NaOH. The formed colored products were kept with stirring in ice bath for 2 h. The coloured products were then filtered off, rinsed by distilled water, and air-dried. Structures of the two ligands **H₂TNBS** and **H₂INBS** are given in Fig. 1.

2.3. Synthesis of copper (II) chelates

For synthesis of Cu complexes, 1 mmol of **H₂TNBS** and **H₂INBS** ligands were dissolved in 40 ml MeOH solvent followed by the addition of just drops of (C₂H₅)₃N base. To this solution, 0.002 mol of the Cu salts; CuCl₂·2H₂O, Cu(CH₃COO)₂·H₂O or Cu(NO₃)₂, solubilized in 20 ml of hot MeOH was slowly added. Precipitation took place once all the amount of the metal salt solution has been added. The obtained coloured precipitates were isolated from solutions by filtration, washed by hot methanol solution and left to dry using vacuum desiccator.

2.4. Antimicrobial evaluation

Antimicrobial tendency of the target compounds were evaluated contra the strains *Staphylococcus aureus* (S. aureus), *Bacillus cereus* (B. cereus), *Escherichia coli* (E. coli), *Salmonella typhi* (S. typhi), *Aspergillus flavus* (A. flavus), and *Candida albicans* (C. albicans). The applied procedures in detailed are shown as supporting data (part S2).

2.5. Antitumor evaluation

The compound under interest in the current study were also examined for their antitumor activity contra the human lung

cancer cells (A-549) and Pancreatic carcinoma (Panc-1) following the method that reported in literature (Mosmann, 1983; Riyadh et al., 2015). Full description of the methods applied for such test are given as supporting data (Part S3).

2.6. Catalytic oxidation of o-aminophenol (OAP)

The synthesized complexes (**1–6**) have been applied to investigate their catalytic performance as phenoxazinone synthase using o-aminophenol as the substrate. The initial rate method was utilized to calculate the reaction rate (Oloyede et al., 2019) while using the reported value of 18300 M⁻¹ cm⁻¹ as the molar absorptivity of the oxidation product (i.e. 2-aminobenzoxazine-3-one) to calculate the initial rate (Gasque et al., 2018; Podder and Mandal, 2020). Details about the instrument, concentrations and work strategy have been depicted in section S4 in the supplementary file.

3. Results and discussion

3.1. Ligands' structure

3.1.1. Mass spectra

Electron impact (EI) mass spectra of the two ligands **H₂TNBS** (**Z**) and **H₂INBS** (**G**) are given in Figs S1 & S2. As shown in the figures, the molecular ion peaks are apparent at $m/z = 410.49$ and 422.14 for **H₂TNBS** and **H₂INBS**, successively, that were found to be consistent with the theoretical molecular weights of the ligands' suggested structures (calculated molecular weights are 410.47 and 422.46 for **H₂TNBS** and **H₂INBS**, respectively).

3.1.2. ¹H NMR

¹H NMR spectra of **H₂TNBS** and **H₂INBS** assigned in deuterated DMSO solvent and in existence of tetramethylsilane (TMS) internal standard are illustrated in Fig. 2 and S3, respectively.

The spectrum of **H₂TNBS** shows singlet at 15.77 ppm that assigned to the phenolic OH proton. The two singlet signals at, 12.8 and 9.71 ppm are assigned to sulfonamide OH and NH protons, respectively, and hence supports the coexistence of the ligand **H₂TNBS** in the two tautomeric structures I and II (Scheme 1) (Kanaani et al., 2016). The peaks located within the range 8.41–6.38 ppm were attributed to the aromatic protons whose integration assuring the existence of the two tautomeric structures I and II (Scheme 1).

For the ligand **H₂INBS**, the singlet appearing at 9.9 ppm assigned to NH proton. The multiple signals appearing within the range 7.59–6.35 ppm have been integrated for the aromatic protons whereas the two singlet signals assigned to the 2 methyl protons appeared at 2.04 and 1.65 ppm (El-Ghamry et al., 2022).

3.2. Complexes structures

3.2.1. Stoichiometry and general composition

on the basis of elements content data and molar conductance values, the empirical formulae of the generated chelates and the two synthesized ligands are displayed in Table 1 together with information of formula weights, color, and melting tem-

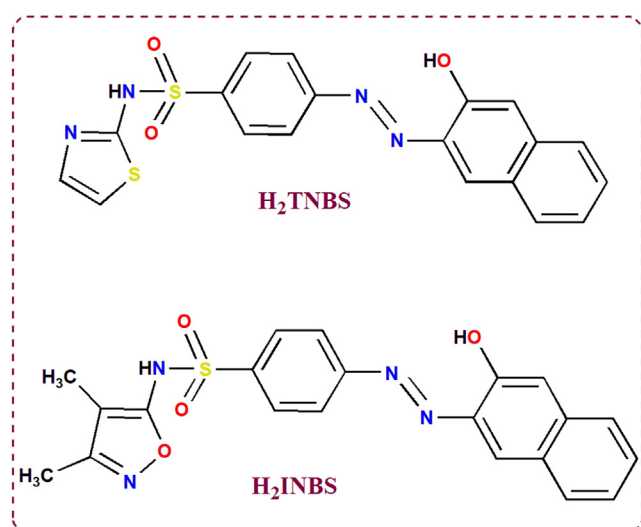


Fig. 1 Structure of **H₂TNBS** and **H₂INBS** ligands.

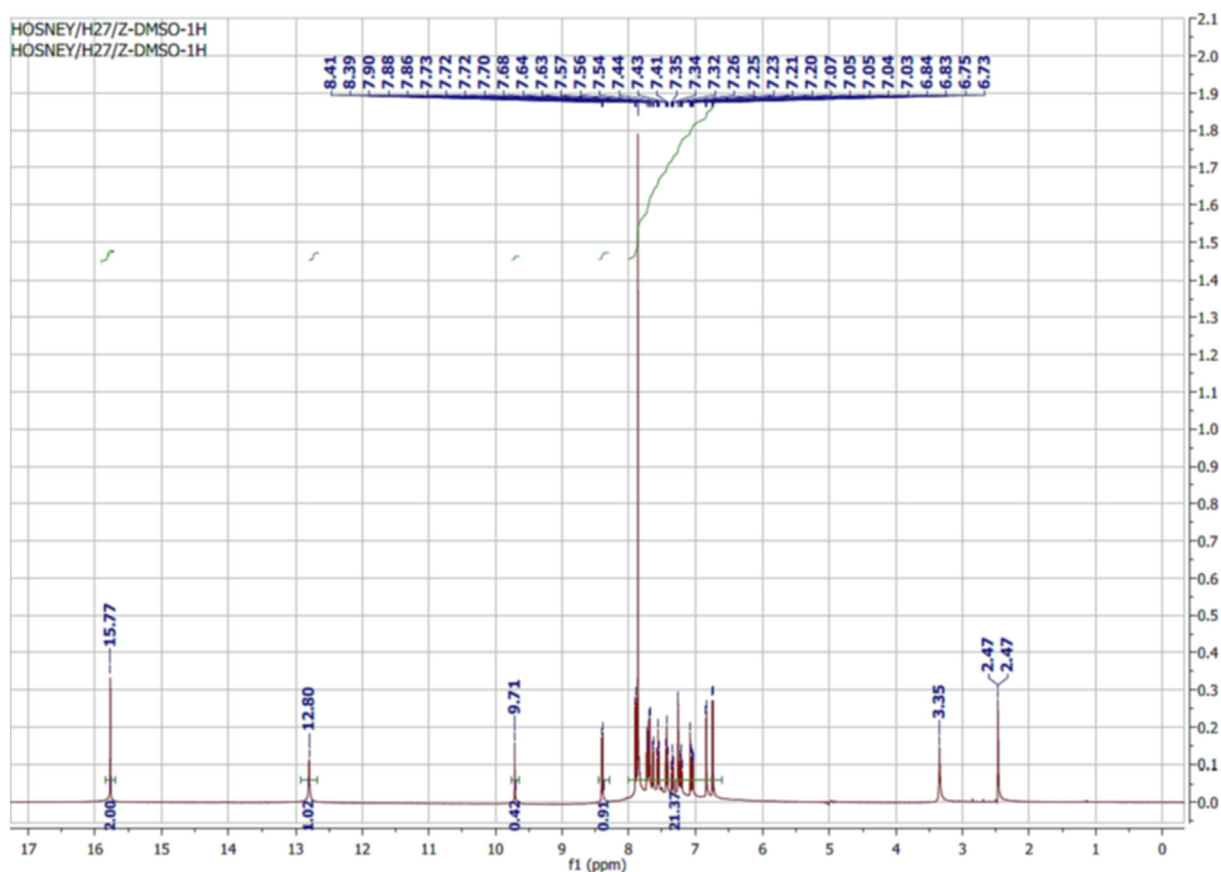
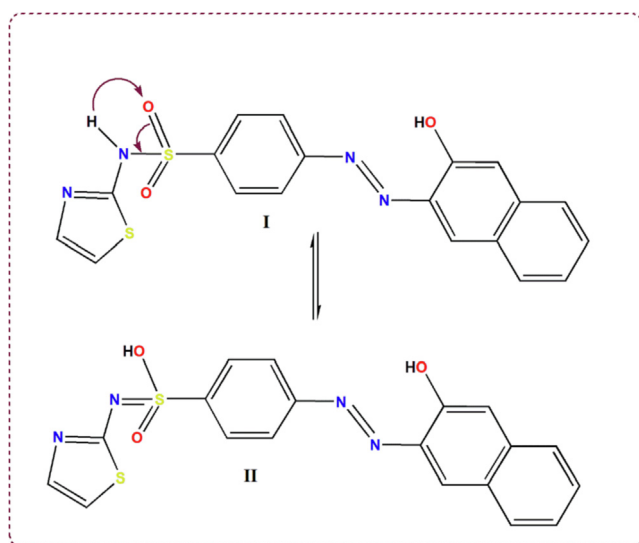


Fig. 2 ^1H NMR spectrum of Structure of H_2TNBS ligand.



Scheme 1 The two tautomeric structures (I and II) of the ligand H_2TNBS .

peratures. The values of elements' percent, which also completely consistent with the data indicated in Table 1, validated the separated chelate structures. Accordingly, these Cu chelates were assured to be produced in a 2: 1 (metal: ligand) ratio for complexes 1–3 and 1:1 for complexes 4–6. From molar con-

ductivity values (measured using 10^{-4} M in DMSO) which found to be inside the range $8.63\text{--}35.6 \Omega^{-1}\text{cm}^2\text{mol}^{-1}$ range supported non-electrolytic complexes formation (Geary, 1971; Fawzy et al., 2020). It was also shown that the complexes maintained their stability despite prolonged subjection to air. Solubility tests demonstrated the ease solubility of all compounds in DMF and MDSO however, in other polar and non-polar solvents, they provided either poor solubility or total insolubility.

3.2.2. EI- mass spectra

Since mass spectrometry offers appropriate spectral analysis to establish the molecular weights and, in turn, the molecular formulae of the synthetic compounds, it has been used to evaluate the acquired Cu(II) complexes, 1–6. The mass spectra of complexes 1–6 are shown in Figs. 3, 4, and S4–S7. These figures show that the molecular ion peaks for complexes 1–6 are observed at $m/z = 657.98, 689.25, 659.19, 538.12, 562.75,$ and 564.43 , respectively. These molecular ion peaks are consistent with the calculated molecular weights of $660.93, 689.66, 659.56, 538.64, 562.05,$ and 565.02 (excluding lattice H_2O molecules) for complexes 1–6, successively.

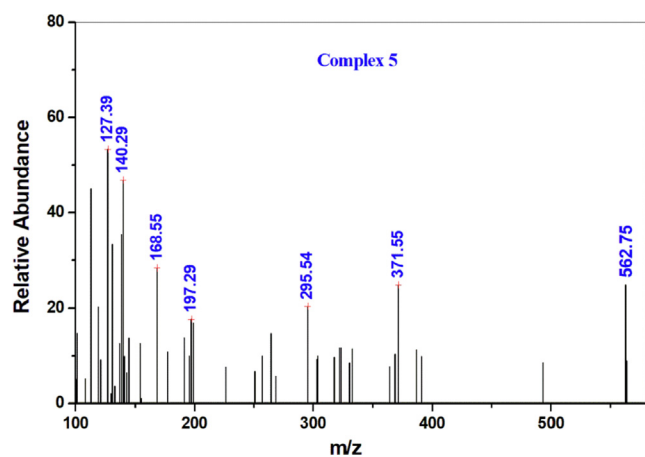
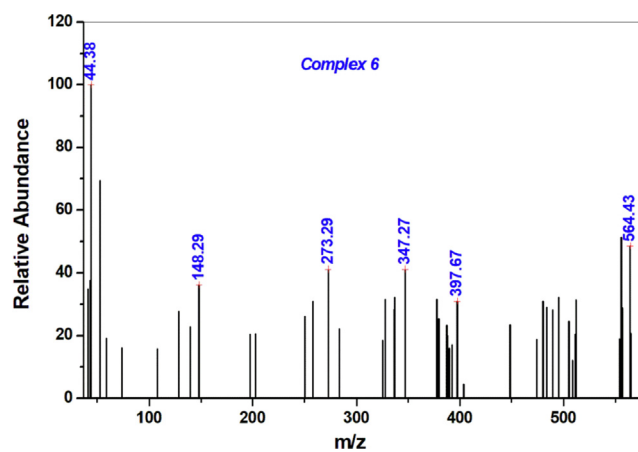
3.2.3. Infrared spectra

The coordinated function groups in the ligand with the metal ions can be determined from the IR spectra of both of them upon comparison with each other, making FTIR spectral anal-

Table 1 The molecular weights, microanalysis data, colours, molecular formulae, empirical formulae, and molar conductance data of **H₂TNBS**, **H₂INBS** and their metal chelates (**1–6**).

No.	Molecular formula (Empirical formulae)	M.p. (°C) (M. Wt.)	Colour (Λ_m)	Microanalysis Found (Calc.) %			
				%C	%H	%N	%M
H₂TNBS	H₂TNBS (C ₁₉ H ₁₄ N ₄ O ₃ S ₂)	235 (410.47)	Orange (-)	55.78 (55.60)	3.62 (3.44)	13.71 (13.65)	–
1	[Cu ₂ (HTNBS)(H ₂ O)Cl ₃].0.5H ₂ O (C ₁₉ H ₁₆ Cl ₃ Cu ₂ N ₄ O _{4.5} S ₂)	Over 300 (669.94)	Reddish brown (9.19)	34.18 (34.06)	2.66 (2.41)	8.51 (8.36)	18.78 (18.97)
2	[Cu ₂ (HTNBS)(OAc) ₂ (H ₂ O) ₂].0.5CH ₃ OH (C _{23.5} H ₂₄ Cu ₂ N ₄ O _{9.5} S ₂)	Over 300 (705.69)	Brown (8.63)	40.22 (40.00)	3.67 (3.43)	7.83 (7.94)	18.32 (18.01)
3	[Cu ₂ (HTNBS)(NO ₃) ₂].H ₂ O (C ₁₉ H ₁₄ Cu ₂ N ₆ O ₁₀ S ₂)	Over 300 (677.57)	Deep brown (20.00)	33.74 (33.68)	2.19 (2.08)	12.61 (12.40)	18.66 (18.76)
H₂INBS	H₂INBS C ₂₁ H ₁₈ N ₄ O ₄ S	166 (422.46)	Faint brown (-)	59.91 (59.70)	4.47 (4.29)	13.43 (13.26)	–
4	[Cu(HINBS)(H ₂ O)Cl].0.5H ₂ O (C ₂₁ H ₂₀ ClCuN ₄ O _{5.5} S)	Over 300 (547.47)	Reddish black (12.60)	47.22 (46.07)	3.84 (3.68)	10.42 (10.23)	11.85 (11.61)
5	[Cu(HINBS)(OAc)(H ₂ O)] (C ₂₃ H ₂₂ CuN ₄ O ₇ S)	Over 300 (562.05)	Deep brown (7.42)	49.30 (49.15)	3.84 (3.95)	9.86 (9.97)	11.54 (11.31)
6	[Cu(HINBS)(NO ₃)(H ₂ O)].H ₂ O (C ₂₁ H ₂₁ CuN ₅ O ₉ S)	Over 300 (583.03)	Faint brown (35.6)	43.21 (43.26)	3.84 (3.63)	12.24 (12.01)	11.16 (10.90)

The yields were found to be 75 %–80 %, Λ_m is the molar conductance ($\Omega^{-1} \text{ cm}^2 \text{ mol}^{-1}$).

**Fig. 3** Mass spectrum of complex 5.**Fig. 4** Mass spectrum of complex 6.

ysis an important tool for characterizing the structure of metal complexes. Distinctive function groups are shown in [Table 2](#) along with their vibration wavenumbers.

This comparison inferred that the two spectral bands occurring at 1499 and 1208 cm^{-1} in the spectrum of **H₂TNBS (Z)** and at 1452 and 1207 cm^{-1} in the spectrum of **H₂INBS (G)** which assigned to the vibration wavenumber of N = N and C-O groups have been shifted to higher or lower values in the spectra of all complexes (**1–6**) by at least 7 cm^{-1} and hence ensuring their incorporation in connection to the copper ion centers in metal complexes ([Khedr et al., 2019](#); [Khedr et al., 2022](#)). The azomethine groups' stretching wavenumbers of thiazole and isoxazole rings appeared in the ligands' **H₂TNBS (Z)**

and **H₂INBS (G)** spectra at 1568 and 1552 cm^{-1} , respectively. The first band has been shifted to lower position in the spectra of complexes **1–3** compared with **H₂TNBS (Z)** ligand whereas the second band appeared in complexes' **4–6** spectra in a position very close to its position in the spectrum of ligand **H₂INBS (G)** assuring that the C = N shared in complex formation in complexes **1–3** but in contrast this band kept free in the spectra of complexes **4–6**. Similarly, the great shift in the position of the of asymmetric and symmetrical vibrations of SO₂ group in the spectra of complex **1** confirm the involvement of its oxygen atom in complex formation while in complexes **4–6**, such group has been confirmed to remain free due to its appearance almost at the same wavenumber as in the ligand **H₂INBS** spectra. Vanishing of SO₂ bands in spectra of com-

Table 2 Assignments of important vibrational spectral bands of H_2TNBS , H_2INBS and their metal chelates (1–6).

Comp.	$\nu(\text{OH})$	$\nu(\text{NH})$	$\nu(\text{C} = \text{N})_{\text{ring}}$	$\nu(\text{N} = \text{N})$	$\nu(\text{SO}_2)$	$\nu(\text{C}-\text{O})$	$\nu(\text{M}-\text{O})$	$\nu(\text{M}-\text{N})$
H_2TNBS	3426	3146	1568	1499	1326, 1127	1208	–	–
1	3416	3114	1549	1461	1374, 1139	1201	558	453
2	3382	–	1543	1463	–	1195	561	449
3	3379	–	1547	1452	–	1180	557	450
H_2INBS	3368	3235	1552	1452	1347, 1164	1207	–	–
4	3381	3191	1550	1442	1346, 1162	1185	577	481
5	3423	3205	1553	1474	1344, 1164	1185	575	426
6	3406	3217	1550	1474	1346, 1162	1182	527	461

Table 3 Electronic absorption spectral results and magnetic moment values of complexes 1–6.

Complex	Wavelength (nm)	Geometry	μ_{eff} (B.M.)
1	282, 315, 374, 416, 493, 738	Square planar	2.41*
2	277, 309, 360, 395, 503, 733	Square planar	2.56*
3	277, 311, 343, 401, 503, 735	Square planar	2.38*
4	251, 310, 392, 498, 710	Square planar	1.81
5	369, 348, 390, 406, 495, 707	Square planar	1.77
6	258, 315, 370, 392, 495, 701	Square planar	1.79

* $\mu_{\text{eff}} / 2\text{Cu}$ centers.

pounds **2** and **3** is explained by coordination of sulfonamide O to the Cu center in the deprotonated enolic form. The non-ligands bands appearing between 558 and 527 cm^{-1} and between 481 and 426 cm^{-1} have been assigned to stretching wavenumbers of Cu–O and Cu–N bonds, successively.

In addition, analysis of the IR spectra allows a precise assignment of the coordinated anion's method of binding to the metal center. The two non-ligand bands that are shown in the spectra of the acetate-containing complexes **2** and **5** have appeared at 1593 and 1341 cm^{-1} for complex **2** and at 1588 and 1351 cm^{-1} for complex **5** and attributed to the $\nu(\text{COO}^-)_{\text{asy}}$ and $\nu(\text{COO}^-)_{\text{sym}}$, respectively, of CH_3COO groups. The difference between $\nu(\text{COO}^-)_{\text{asy}}$ and $\nu(\text{COO}^-)_{\text{sym}}$ has been calculated and equals 252 and 237 cm^{-1} , matching with the $\Delta\nu$ value reported for monodentate acetate groups (Olar et al., 2013).

For **3** and **6** (containing NO_3 coordinating groups), the two bands occurring at 1427 & 1297 cm^{-1} in complex **3** spectrum and at 1402 & 1216 cm^{-1} for complex **6** with $\Delta\nu$ differences of 130 and 186 cm^{-1} , successively, assured the bi- and unidentate ligation fashion of nitrate groups in complex **3** and **6**, successively (Takroni et al., 2020).

3.2.4. Magnetic moment

Cu(II) complexes **1–3** were discovered to have magnetic moment values that fell within the range of 2.38–2.56 B.M. for the two Cu(II) centers (Table 3). Such values are quite close to the calculated one corresponding to bimetallic chelates with two Cu(II) centers that are not in interaction (i.e. 2.45 B.M.) (Li and Jin, 2009).

For complexes **4–6**, the magnetic moment values were measured to be 1.77, 1.79 and 1.81 B.M., respectively, which are almost within the acceptable spin-allowed limit for a single

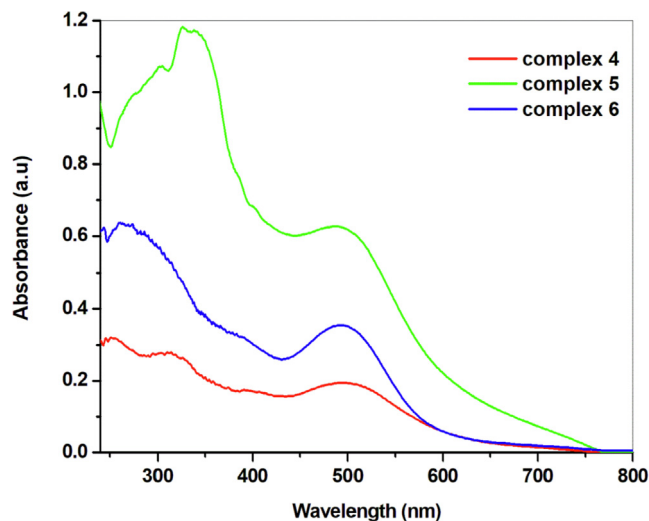


Fig. 5 UV-Vis spectra of compounds **5–8** using nujol mull technique.

electron (i.e. 1.73 B.M.) in mononuclear Cu(II) chelates (Takroni et al., 2020).

3.2.5. Electronic spectra

The most important study for identifying geometry of the ligand atoms surrounding the core metal ion in metal chelates is the electronic absorption spectra (UV-Vis). Accordingly, the nujol-Mull method was used to measure the UV-Vis spectra of compounds **1–6** over the wavelength range of 200–800 nm.

In all complexes' spectra, Figs. 5, S8 and Table 3, the bands appearing within the ranges 251–282, 209–348 and 360–392 nm with medium to high absorbance are characteristic for $\pi \rightarrow \pi^*$ transitions of benzene ring, $\pi \rightarrow \pi^*$ and $n \rightarrow \pi^*$ transitions in C = N & N = N groups, respectively (Yarkandi et al., 2017). The broad bands apparent in 493–503 nm range assigned to LMCT (Cadranel et al., 2017).

The low and broad intensity bands apparent in the spectra of six complexes in the range 707–738, has been assigned to ${}^2\text{B}_{1g} \rightarrow {}^2\text{A}_{1g}$ transition familiar for square planar architectures (Uysal and Kurşunlu, 2011).

3.2.6. Thermogravimetric analysis (TGA)

The thermogravimetric (TGA) analytical tool is one of the useful instruments that is frequently used to gain understanding of the structure and stability of inorganic compounds. The full

analysis of the TG thermograms of complexes **1–6** along with the derivative thermogravimetric data (DTG) the is shown in Figs. 6 & S9 and interpreted in Table 4.

Compounds **1–6** underwent disintegration in three decomposition ranges as for complexes **5** and **6**, four decomposition ranges as in the complexes **1** and **3** or five decomposition ranges as in the complexes **2** and **4**.

A closer look at the results given in Table 4 revealed that only lattice or lattice and coordinated water molecules are lost during the first stage of disintegration, which began at ambient temperature and continued up to 150 °C. The next step of decomposition occurred between 72 and 403 °C, inside which coordinated water or anions get lost in some compounds. The subsequent steps of breakdown are attributed to the progressive breakdown of the organic ligand molecules included in the complexes' structures. Table 4 also lists and illustrates the DTG temperatures for each stage. The following Scheme (Scheme 2) also indicate the thermal decomposition of complexes **1** and **2**, as example:

3.2.7. X-ray diffraction investigations

In light of current advancements in material science technology and knowledge, X-ray diffraction (XRD) is considered as one of the most significant and frequently employed material characterization technique. It is commonly applied to gather structural information on chemical compounds' micro-crystalline structures in the solid state (Ali et al., 2022). As a

result, the diffraction patterns of organic ligands **H₂INBS** & **H₂TNBS** and inspected metal complexes (**1–6**) were implemented within $10^\circ < 2\theta > 80^\circ$ scattering angle range (Figs. 7 & S10). The ligands' diffraction patterns allocations are drastically distinct from those of the equivalent metal complexes, which supports complex formation and shows that there are no contaminants or beginning reactants that are smeared (Khedr et al., 2022). The acquired x-ray diffraction patterns denoted that ligand **H₂TNBS** displayed high crystallinity with diffraction patterns totally distinct from those of complexes **1–3** which exhibited good to weak crystallinity. Also, high crystallinity afforded for ligand **H₂INBS**, good crystallinity of complex **4** and weak crystallinity of complex **5**, with completely different diffraction patterns, whereas complex **6** is fully amorphous. Depending upon the Deby-Scherrer equation calculations (Sanad et al., 2022), the average crystallite sizes have been calculated:

$$\tau = \frac{K\lambda}{\beta \cos\theta}$$

where, τ is the mean size (crystallite size) of the ordered (crystalline) domains, which may be smaller or adequate to the grain size, λ is the X-ray wavelength, K mean a dimensionless shape factor and its value amounts to unity (0.9), but varies with the actual shape of the crystallite, β refers to line broadening at half the maximum intensity (FWHM), after subtraction of the instrumental line broadening.

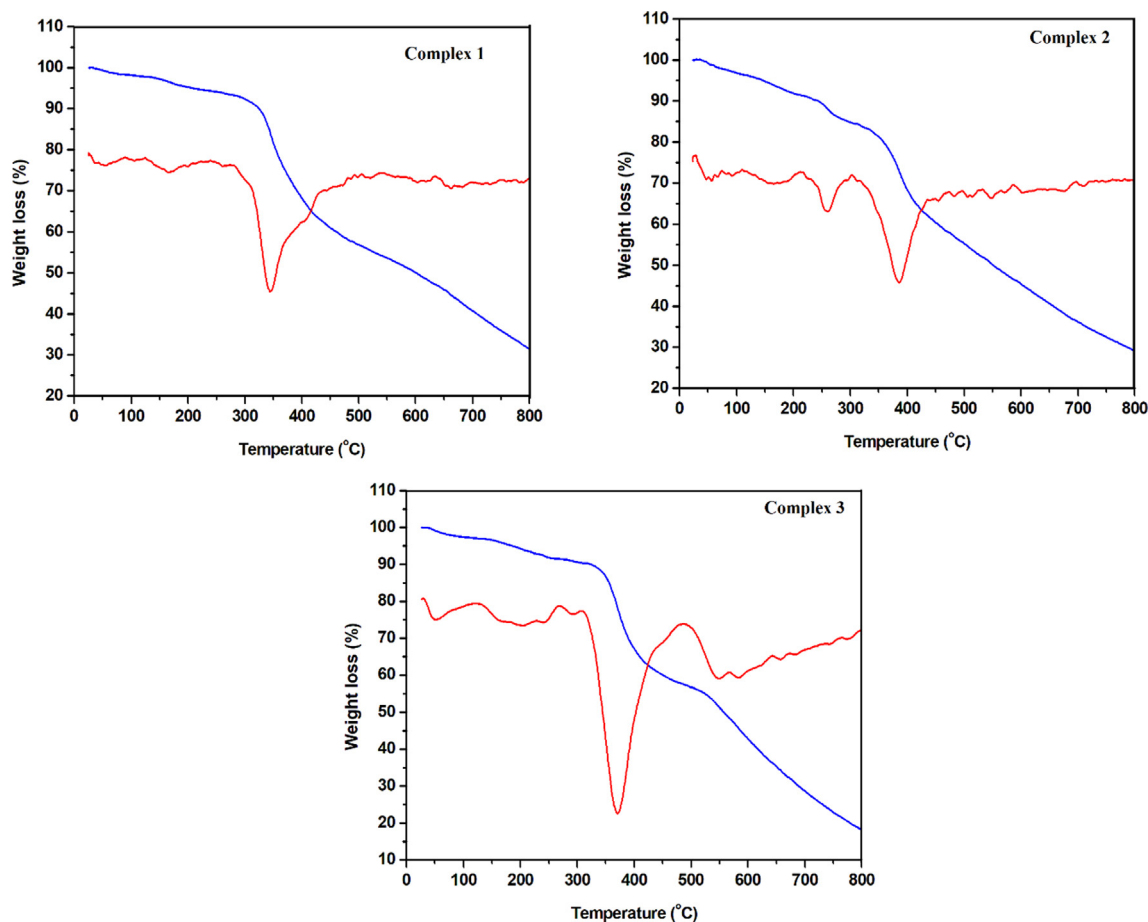


Fig. 6 TG/DTG thermograms of complexes **1–3**.

Table 4 Thermal analysis results interpretation of complexes 1–6.

Complex (Mol. Wt.)	Temp. range (°C)	Mass loss %		DTG (°C)	Assignment
		Calcd	Found		
1 [Cu ₂ (HTNBS)(H ₂ O)Cl ₃]. 0.5H ₂ O (669.94)	25–84	1.34	1.67	60	-Loss of 0.5 lattice H ₂ O.
	84–180	2.68	2.49	164	-Loss of 1 coordinated H ₂ O.
	180–483	37.66	37.65	345, 410	-Loss of 1.5Cl ₂ + C ₃ H ₃ N ₂ OS ₂ .
	483–800	Not assigned	26.37	668	- Not assigned.
2 [Cu ₂ (HTNBS)(OAc) ₂ (H ₂ O) ₂]. 0.5CH ₃ OH (705.69)	25–72	2.27	2.26	54	-Loss of 0.5 lattice CH ₃ OH.
	72–185	5.10	5.05	169	-Loss of 2 coordinated H ₂ O.
	185–305	8.36	8.09	259	-Loss of 1CH ₃ COO group.
	305–436	23.11	22.81	385	-Loss of 1CH ₃ COO group + C ₆ H ₄ N ₂ .
	436–800	Not assigned	32.86	–	- Not assigned.
3 [Cu ₂ (HTNBS)(NO ₃) ₂].H ₂ O (677.57)	25–97	2.65	2.67	48	-Loss of lattice H ₂ O.
	97–304	6.79	6.85	162, 204	-Loss of NO ₂ group.
	304–449	30.72	30.61	371	-Loss of NO ₂ group + C ₃ H ₂ N ₂ O ₂ S ₂ .
	449–800	Not assigned	42.28	550	- Not assigned.
4 [Cu(HINBS) (H ₂ O)Cl].0.5H ₂ O (547.47)	25–92	1.64	1.91	69	-Loss of 0.5 lattice H ₂ O.
	92–234	17.26	17.81	139, 195 213	-Loss of 1 coordinated H ₂ O + 0.5Cl ₂ + C ₂ H ₃ N.
	234–302	10.05	10.11	283	-Loss of C ₃ H ₃ O.
	302–436	14.44	14.19	334	-Loss of SO ₂ NH.
	436–800	19.01	19.92	654	-Loss of C ₆ H ₄ N ₂ .
5 [Cu(HINBS) (OAc)(H ₂ O)] (562.05)	25–150	3.20	3.15	86	-Loss of 1 coordinated H ₂ O.
	150–403	50.05	50.28	281	-Loss of CH ₃ COO + C ₁₀ H ₆ + C ₇ H ₆ N ₂ O.
	403–800	Not assigned	22.72	458	- Not assigned.
6 [Cu(HINBS) (NO ₃)(H ₂ O)].H ₂ O (583.03)	25–133	6.17	6.43	110	-Loss of 1 lattice and 1 coordinated H ₂ O.
	133–294	19.03	19.33	261	-Loss of C ₅ H ₇ N ₂ O moiety.
	294–715	39.48	39.65	358	- Loss of NO ₃ group + C ₇ H ₄ N ₂ O ₂ S moiety.

Applying this equation to the obtained spectra, the ligand **H₂TNBS**, complex **1**, complex **2**, and complex **3** exhibited 20.7, 19.0, 5.5 and 16.3 average crystallite sizes, respectively, and ligand **H₂INBS**, complex **4**, and complex **5** found to be 33.7, 25.3 and 8.0 nm, respectively. The irregular arrangement of the materials' particles through their precipitation may be indicated by the complexes' amorphous nature. This amorphous state will predominate if the complexation process is rapid and/or the produced chemical is cooled quickly. Additionally, many of the structural elements of the complex cannot be accommodated in crystalline form. The amorphous compounds with probable small sizes are usually investigated by TEM technique to examine if they are having particles sizes in the nano-metric range. These nanometer-scale compounds usually receive a lot of interest due to their improved functional properties and wide range of potential technological applications, including optics, microelectronics, catalysis, bio- and chemical sensors (Gaber et al., 2017).

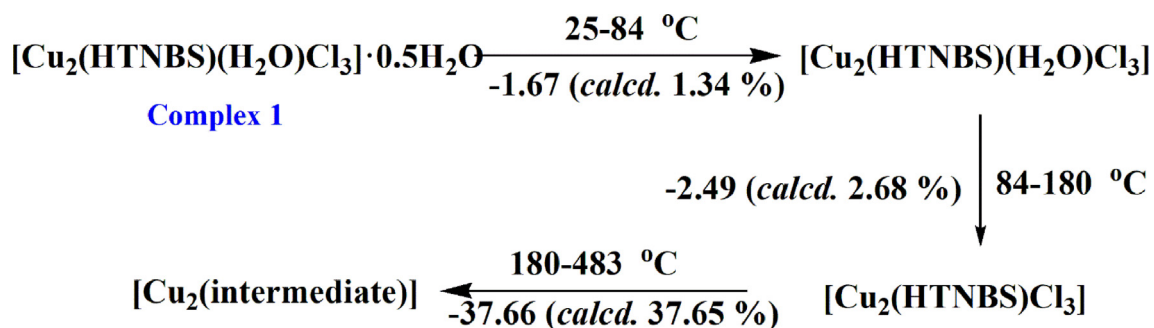
3.2.8. Investigation of TEM images

Transmittance electron microscopy (TEM) is one of the most common techniques to study a wide range of fascinating nano-sized materials. It's a method that's usually employed

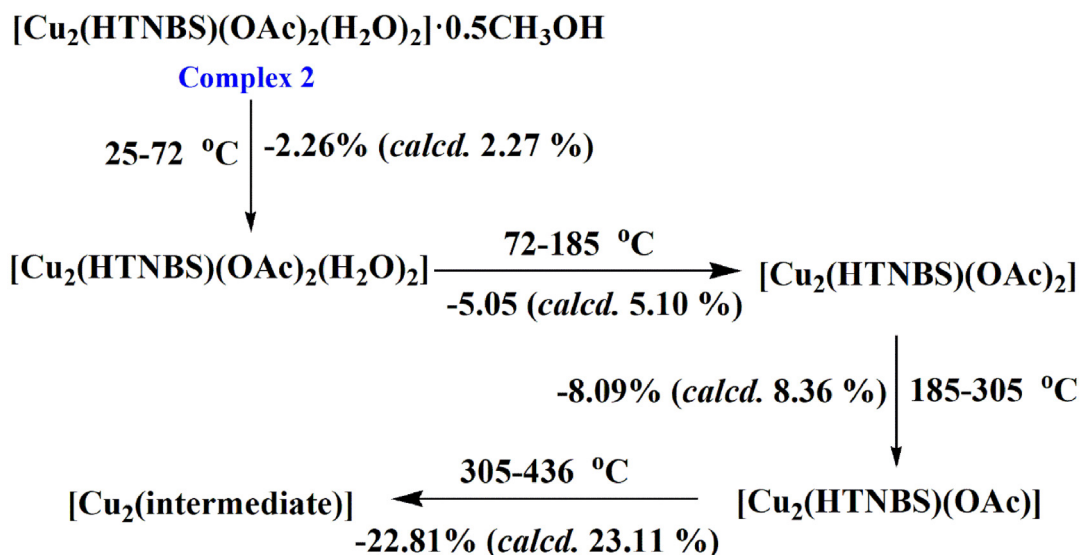
to look at the shape and dimensions of solid materials. Therefore, the particle sizes and crystallinities of the produced complexes **1–6** were further investigated by TEM technique. Images captured by the transmittance electron microscope in bright field for complexes **1–6** are shown in Fig. 8 & S11–S14 demonstrating that the samples are made up of teeny, different-sized nanoparticles. These photos make it abundantly notable that the complexes powders are made up of nanoscale particles with spherical-like shape (either regular or not). Additionally, it was determined that the particle size of metal complexes ranged between 15.9 and 45.6 nm for example complex **1** and 27.89–39.37 nm for **2** while complex **3**'s was 18.19–34.12 nm, complex **4**'s was 9.48–23.25 nm, complex **5**'s was 12.13–18.45 nm and complex **6**'s was 13.80–20.63 nm.

Accordingly, in comparison to their bulk analogues, the biological effectiveness of these innovative synthetic compounds is suspected to be stronger at these nanometric scales. There is a lot of interest that might be sparked by the novel functional properties of the nanosized chelates and the wide range of potential uses (Saad et al., 2019).

As a result, and in light of all the investigations previously deliberated, the structures of compounds **1–6** are depicted in Figs. 9 and 10.



Decomposition stages of complex 1



Decomposition stages of complex 2

Scheme 2 Decomposition stages of complexes 1 and 2.

3.3. Applications

3.3.1. Antimicrobial investigation

As described in the experimental part, the examined two ligands, H_2TNBS and H_2INBS , and their complexes (1–6) were subjected to antimicrobial screening applying a well diffusion method (Jahangirian et al., 2013) (Table 5). All inspected compounds displayed very strong and promising against *S. aureus* within inhibition zones ranged from 15 to 26 mm which are higher than the inhibition zone of the used standard Gram-positive ant-bacterial agent Amoxycillin-clavulanic (10 mm) by one and half to two and half. Also, the inhibition zones of examined ligands and complexes towards *B. cereus* varied from 12 to 28 mm, which exceeds the inhibition zone of standard Gram-negative antibacterial agent (12 mm) by two and half times of value. Complexes 1, and 5 exhibited inhibition zones equal 9 equivalent to that of the standard bactericide (8 mm) against *E. coli*, whereas complexes 2 showed 19 mm, more than

the double value of the common standard towards the same organism, respectively. Complex 4, displayed antibacterial activity (16 mm) double that of the applied standard (8 mm) against *S. typhi*. At the same time, ligand H_2TNBS and complex 3 showed 12 and 9 mm inhibition zones towards it. Only ligand H_2INBS showed excellent antifungal activity against the multicellular fungus *A. flavus*, with 26 mm inhibition zone which is higher than double the value of applied standard fungicide (11 mm). Ligands H_2INBS and H_2TNBS exhibited inhibition zones 16 and 12 mm against *C. albicans*. Upon complexation the inhibition zones of complexes 3 and 5 increased compared with the corresponding ligands and arrived 16 and 18 mm. These values are equivalent or greater than the standard Amphotericin-p (13 mm) towards the same unicellular fungus. The selected species demonstrate diversity of microorganisms, including Gram-positive and Gram-negative bacteria, unicellular and multicellular fungus (Khedr et al., 2022). In most instances, the increased antibacterial effect during chelate

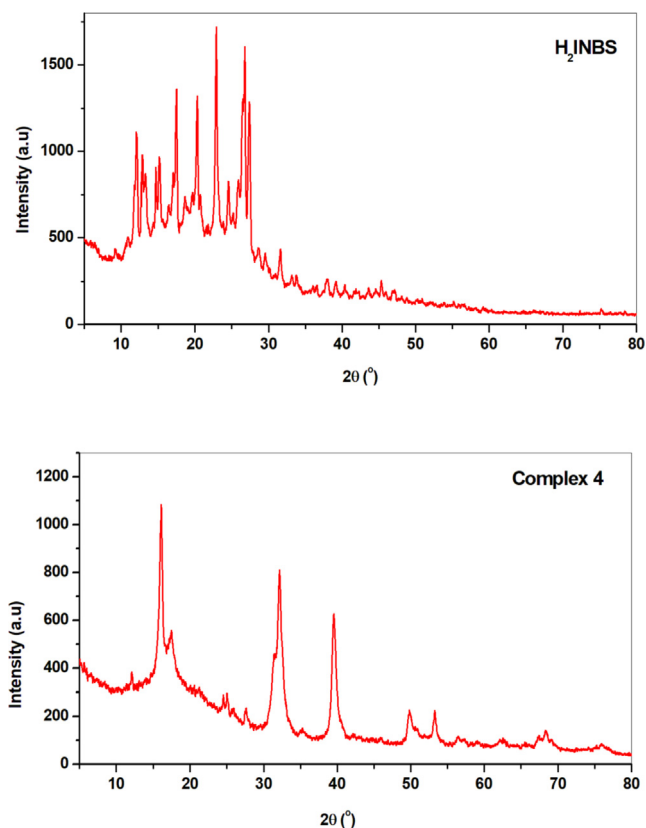


Fig. 7 XRD spectra of H_2INBS complex 4.

formation can be ascribed to metal ions existence, with more hyper sense to microbial cells than the chelating ligands (Saad et al., 2017). Moreover, the greater action of the metal chelates may be caused by the increased lipophilicity during complexation. The coordinated metal ions may cause detrimental interactions between cellular components, or they

may stop cellular enzyme activity. Obvious variation in the efficacy of the alternative compounds under study contra distinct organisms are brought on either by the impermeability of the cells of microorganisms or variations in the ribosomes in microbes' cells (Singh et al., 2007). Additionally, Overton's notion and Tweedy's chelation hypothesis offer the greatest explanations for this improved efficiency upon complex development (Saad et al., 2019). According to the available information, the studied ligands and their complexes hold a great deal of promise for becoming broad-spectrum, novel, highly effective, fungicides and bactericides.

3.3.2. Performance as antitumor agents

The vast number of cytotoxic chemicals that are currently available includes a significant number of metal-based complexes. Platinum (II) complexes, such as cisplatin, oxaliplatin, and carboplatin, which are particularly target genomic DNA are frequently utilized in clinical settings to treat a variety of malignancies. In about 50% of chemotherapy-treated cancer patients, either alone or in combination, a platinum medication is administered. Despite playing a key role in cancer chemotherapy, platinum medicines have significant limitations, including a narrow range of antitumor activity, systemic dose-related toxicity, and a propensity to induce drug resistance, which frequently results in treatment failure (Gamberi and Hanif, 2022). The exploration of nonplatinum metal-based medications as an efficient substitute has sparked a great interest in response to these observations (Saad et al., 2018). In this regard, we seek to evaluate the antitumor efficacy of azo ligands H_2TNBS & H_2INBS and their chelates (1–6) against human Lung carcinoma (A-549) and Pancreatic carcinoma (Panc-1) and cells (Table 6 and Fig. 11). Untreated cells used as a control and vinblastine sulphate (VS) as a reference drug which had IC_{50} values of 4.68 and 24.6 and $\mu\text{g}/\text{ml}$ contra pancreatic and lung cancer cell lines, respectively. The inspected compound concentration that caused 50% decrease in cell reproduction are referred IC_{50} . IC_{50} is defined as the concen-

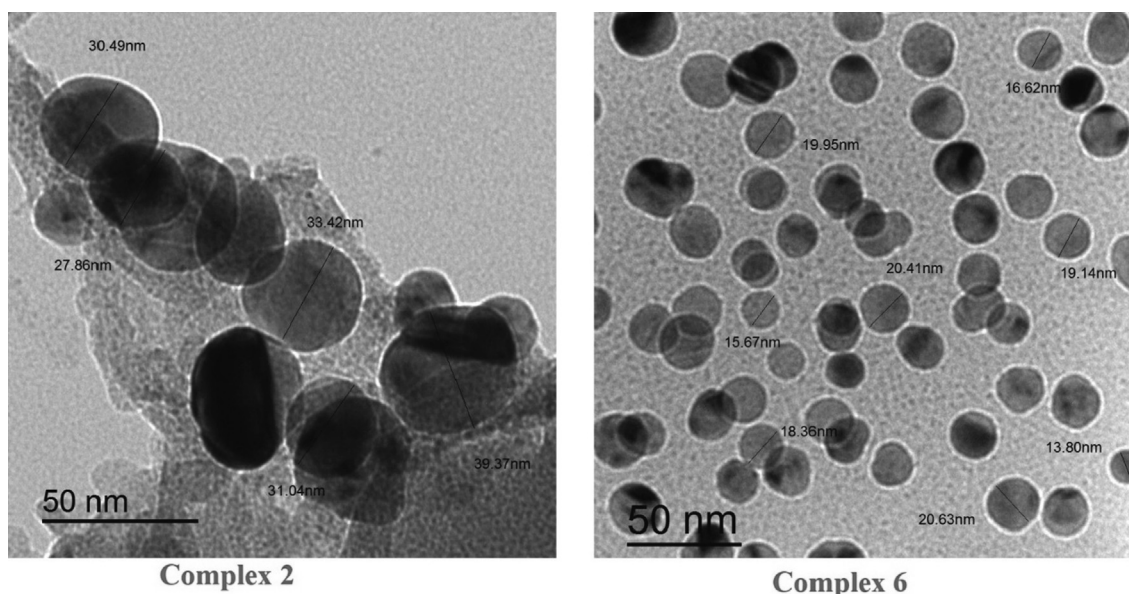


Fig. 8 Compounds 2 and 6 TEM images.

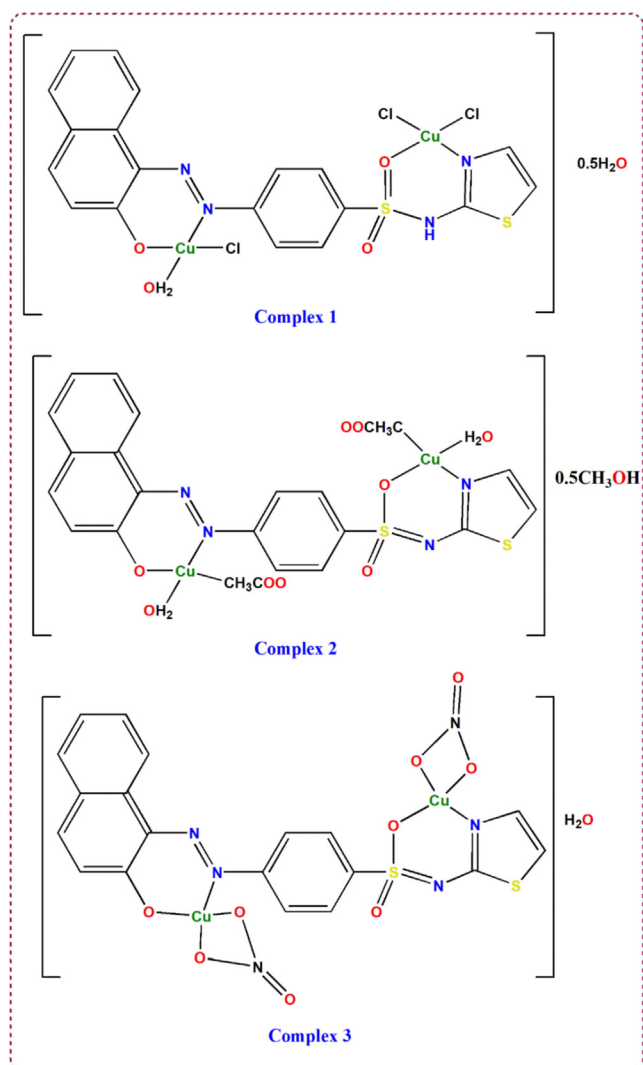


Fig. 9 Concluded structures for complexes 1–3.

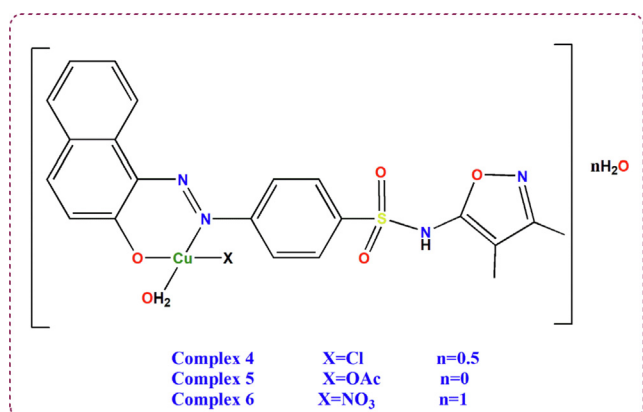


Fig. 10 Concluded structures for complexes 4–6.

tration that, under usual conditions, inhibits cell growth by 50%. The average of three separate experimental repetitions is averaged to produce each final value (Khedr et al., 2019). The obtained data made obvious that inspected compounds

exhibited an increasing propensity to colonies lung cancer cell lines; $H_2TNBS < H_2INBS < 6 < 4 < 5 < 1 < 3 < 2$. The examined compounds reduced the viability of cancer cells, which was significantly influenced by their structures, mainly with the type of anions attached to the complex and geometrical arrangement around the core metal ion (Gaber et al., 2018). With IC_{50} values of 10.41, 4.99, 7.44, 19.62, 12.65 and 29.54 $\mu\text{g ml}^{-1}$ for complexes 1–5, respectively, demonstrated strong and very encouraging anticancer actions toward A-549 cells, overcoming the standard vinblastine sulphate having IC_{50} of 24.60 $\mu\text{g ml}^{-1}$. Complex 6 displayed very good anticancer efficiency with IC_{50} equals 29.54 $\mu\text{g ml}^{-1}$, substantially equal to VS against the same tumor cells. Furthermore, an increase in anticancer effectiveness and inhibition of cell viability against Panc-1 were seen for all drugs under consideration in increasing order; $H_2TNBS < H_2INBS < 6 < 4 < 5 < 1 < 3 < 2$. With IC_{50} values of 2.57 and 3.98 $\mu\text{g ml}^{-1}$, respectively, complexes 2 and 3 demonstrated strong and extremely promising anticancer actions toward Panc-1 cells, exceeding the standard drug vinblastine sulphate with IC_{50} equal 4.68 $\mu\text{g ml}^{-1}$. Also, complexes 5 and 1 displayed excellent and encouraging Panc-1 antitumor efficiency within 9.20 and 6.54 $\mu\text{g ml}^{-1}$, IC_{50} value whereas complex 1 showed acceptable IC_{50} (14.23 $\mu\text{g ml}^{-1}$). Depending on these findings, these compounds may undoubtedly be regarded as efficient and potential anticancer therapies for the examined tumor cells.

3.3.3. Effectiveness toward phenoxazinone synthase and kinetic studies

Recording of APX absorption peak that produced consequent to the oxidation of OAP by the power of Cu(II) chelates; 1–6, exhibited a raise of the main peak APX with time. This band emerged in Cu(II) complexes' spectra around 435 nm, and consequently supported their catalytic effect for phenoxazinone synthase like activity. Figs. 12, 13 & S15-S18 show the time dependent spectra of complexes 1–6 with concentration of 3×10^{-5} M with addition of 10^{-2} M of OAP in DMF medium under aerobic condition. For these catalytic reactions, once OAP was added to the complexes' solutions, time started, and the compounds' spectra were recorded each 5 min up to 70 min. When the same experiments were run without catalysts, no observed increase in APX peak was seen (blank test). The observed rate constant (k_{obs}) and the initial rate of reaction (V_0) have been assessed using the initial rate method (Table 7) ($\epsilon_{\text{APX}} = 18300 \text{ M}^{-1}\text{cm}^{-1}$) (Podder and Mandal, 2020).

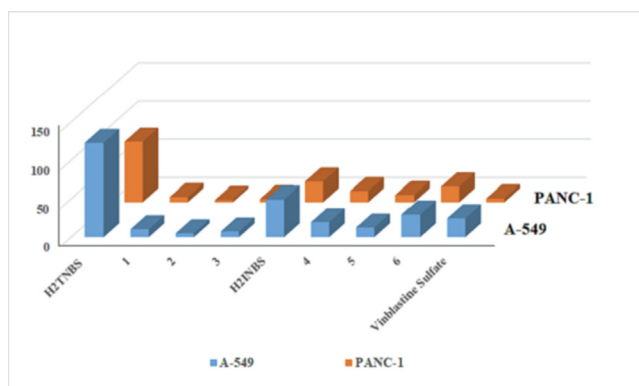
The kinetics of the reactions were studied in order to assign the applied Cu(II) complexes' level of catalytic performance in comparison to one another and to other known comparable compounds. In these reactions, 3×10^{-5} M solutions of each catalyst was treated with series of substrate concentrations (with concentrations in the range $1-8 \times 10^{-3}$ M). The substrate concentration 10 times, at least, higher than the concentration of the catalyst to make sure that pseudo-first order kinetics is applied. For each catalytic solution, the absorption peak of APX, which is formed as the product of substrate oxidation, was taken once the reaction started and each 3 min intervals until the time of the reaction reached 21 min. The recorded absorbances were used to assign the initial rate for each catalytic solution. Plotting the substrate concentrations ($[S]$) versus initial rate (V_0) inferred that the majority of the Cu

Table 5 Antibacterial and antifungal activities of H₂TNBS, H₂INBS and their metal chelates (1–6) applying well diffusion method at 30 °C after 24 h in the form of inhibition zone diameter (mm).

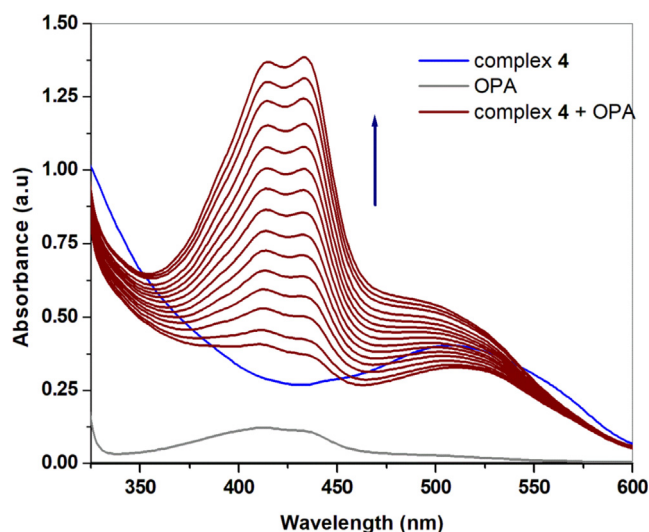
Compound	<i>Staphylococcus Aureus</i>	<i>Bacillus cereus</i>	<i>Escherichia Coli</i>	<i>Salmonella typhi</i>	<i>Aspergillus flavus</i>	<i>Candida albicans</i>
H ₂ TNBS	15	15	–	12	–	12
1	26	22	9	–	–	6
2	25	28	19	–	–	8
3	24	20	–	9	–	16
H ₂ INBS	16	12	–	–	26	16
4	17	24	–	16	–	9
5	22	20	9	2	–	7
6	21	24	–	–	–	18
Amoxicillin-clavulanic (AMC30)	10	12	8	8	–	–
Amphotericin-p	–	–	–	–	11	13

Table 6 The *in-vitro* antitumor activity as IC₅₀ (μg/ml) of H₂TNBS, H₂INBS and their metal chelates (1–6) against A-549 and PANC-1 cell lines.

Compound	IC ₅₀ (μg/ml)	
	A-549 (Human lung carcinoma)	PANC-1 (Pancreatic carcinoma)
H ₂ TNBS	122.5 ± 6.78	78.52 ± 4.78
1	10.41 ± 0.97	6.54 ± 0.65
2	4.99 ± 0.36	2.57 ± 0.17
3	7.44 ± 0.62	3.96 ± 0.23
H ₂ INBS	48.82 ± 3.98	26.59 ± 2.09
4	19.62 ± 0.98	14.23 ± 1.21
5	12.65 ± 0.67	9.20 ± 0.98
6	29.54 ± 0.91	20.09 ± 0.65
Vinblastine Sulfate	24.6 ± 0.65	4.68 ± 0.65

**Fig. 11** The *in-vitro* anticancer evaluation test as IC₅₀ (μg/ml) of H₂TNBS, H₂INBS and their metal chelates (1–6) against A-549 and PANC-1 cancer cells.

complexes under investigation provided rate saturation kinetics (Figs. 14, 15, and S19–S22). The outcomes clearly demonstrate the pre-equilibrium production of the complex-

**Fig. 12** The increase in APX spectral peak at ≈ 435 nm upon addition of 10⁻² M of OAP to 3×10⁻⁵ M of catalyst 4, the reaction medium is DMF.

substrate intermediate, and the irreversible substrate oxidation is the rate-determining stages for catalytic cycle, which eventually developed APX, as demonstrated by the equation:

The applied catalysts afforded saturation kinetics, so Michaelis-Menten equation is the most significant equation for treatment of such reactions. The following equation illustrates the connection between [substrate] (i.e [S]) and the rate of the enzyme reaction (V) using this kinetic-like model:

$$V = \frac{V_{max}[S]}{K_M + [S]}$$

V_{max} is the greatest rate which the system can achieve when [substrate] reaches saturation levels. The Michaelis constant, or K_M , refers to the substrate's concentration at which the reaction rate is half of V_{max} . By linearizing the Michaelis-Menten equation, a double reciprocal Lineweaver-Burk plot is created, which is applied to examine different kinetic parameters like V_{max} and K_M . The formula serves as an example of the Lineweaver-Burk Equation.

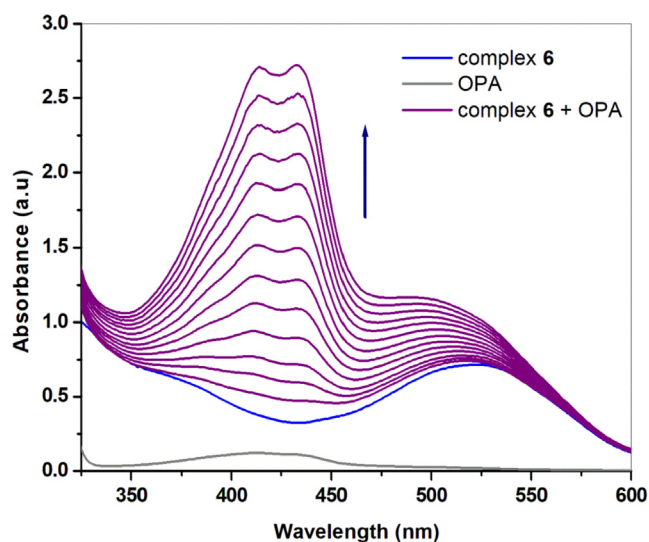


Fig. 13 The increase in APX spectral peak at ≈ 435 nm upon addition of 10^{-2} M of OAP to 3×10^{-5} M of catalyst **6**, the reaction medium is DMF.

$$\frac{1}{[S]} = \frac{K_M}{V_{\max}[S]} + \frac{1}{V_{\max}}$$

Fulfillment of the previous equation to the kinetic process of the examined catalysts (Figs. 14 & 15), result in the calcula-

tion of the kinetic parameters V_{\max} , K_M and the turnover number (k_{cat} , h^{-1}) which are collected in Table 7.

Table 7 shows that H_2INBS chelates (compounds **4–6**) had higher activity than H_2TNBS chelates (complexes **1–3**), indicating that the ligand structure is one of the factors influencing the activity of the complexes.

On comparing the activity of the synthesized catalysts; **1–6**, relatively according to each other, the following remarks can be summarized:

For complexes **1–3**, the catalytic activity of these complexes that deduced from TOF values indicated complex **1** to exhibit the uppermost efficacy with k_{cat} of 60.8 h^{-1} followed by compound **3** having k_{cat} value of 32.15 h^{-1} and finally the least activity afforded by compound **2** with k_{cat} of 4.34 h^{-1} . On the other hand, for H_2INBS chelates; **4–6**, the obtained results showed an extreme activity for compound **6** having 467.01 h^{-1} k_{cat} value and the next is compound **4** having k_{cat} equals 390.48 h^{-1} and the least activity observed for complex **5** having k_{cat} equals of 22.82 h^{-1} .

It is observed that APX generation through oxidation of OAP by the catalytic effect of copper chelates can only take place in existence of molecular dioxygen since there is hardly any peak of APX appears without the availability of O_2 in a similar behavior of reported work (Sohtun et al., 2021; Mandal et al., 2020). The suggested mechanism is shown in Scheme S1 (Sarkar et al., 2017).

Comparing the activity of the metal chelates with each other can lead to conclude that the metal center oxidation

Table 7 Kinetic parameters for phenoxazine synthase like efficacy calculated by applying Michaelis-Menten equation on compounds **1–6**.

Comp. code	$K_{\text{obs}} (\text{min}^{-1})$	$V_o (\text{M min}^{-1})$	$V_{\max} (\text{M min}^{-1})$	$K_M (\text{M})$	$k_{\text{cat}} (\text{h}^{-1})$
1	0.00715	3.91×10^{-7}	3.04×10^{-5}	0.744	60.8
2	0.0034	1.86×10^{-7}	2.17×10^{-6}	0.091	4.34
3	0.0047	2.60×10^{-6}	1.607×10^{-5}	0.593	32.15
4	0.01451	7.93×10^{-7}	1.95×10^{-4}	2.41	390.48
5	0.00298	1.63×10^{-7}	1.14×10^{-5}	0.692	22.82
6	0.0391	2.14×10^{-6}	2.33×10^{-4}	0.973	467.01

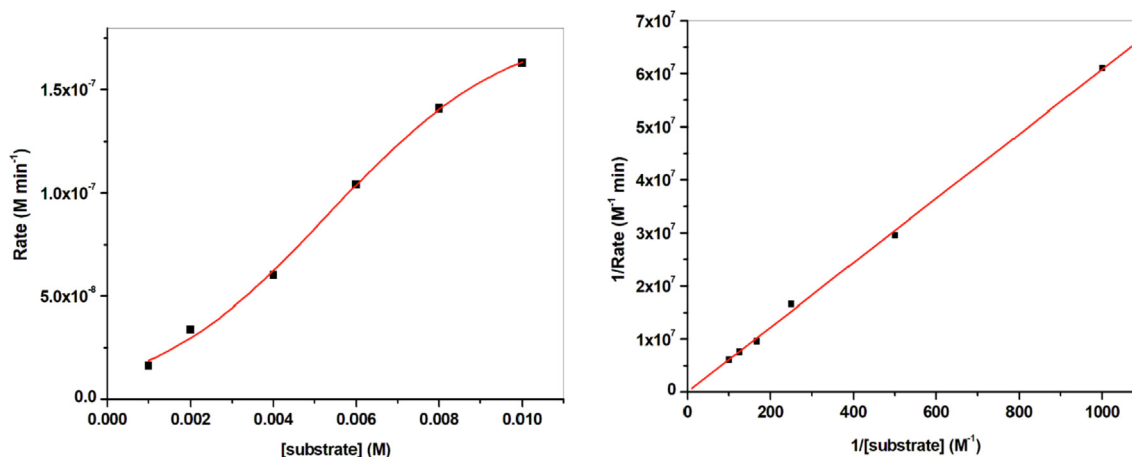


Fig. 14 Michaelis-Menten plot (left) and Lineweaver-Burk plot (right) of complex **5** for catalytic oxidation of OAP.

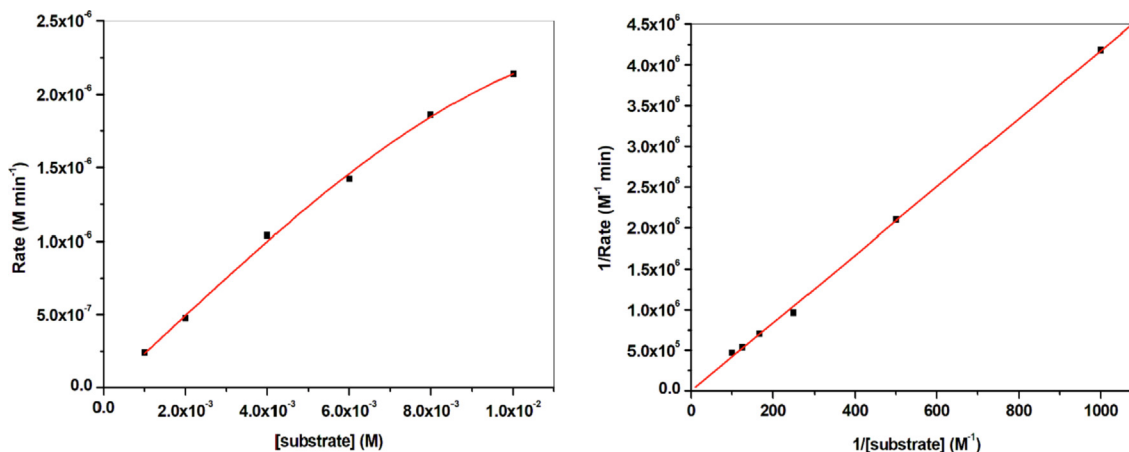


Fig. 15 Michaelis–Menten plot (left) and Lineweaver–Burk plot (right) of complex **6** for catalytic oxidation of OAP.

number and its geometry. The distance between metals in bimetallic center and the structure of organic ligand are also important factors that contributes to catalysts' activity. Comparing the activity of the metal complexes incorporating the same ligand (i.e. compounds **1–3** with each other and compounds **4–6** with each other) inferred that the key factor controlling the activity is the type of incorporated anion sine all the other factors among each group of compounds are the same. Chloro complexes, **1** & **3**, and nitro complexes, **3** & **6**, provided the highest activity whereas the other complexes, which are only weakly active, contain CH_3COO^- anions in their structure (i.e., complexes **2** and **5**). Depending on the approachability of the labile sites in the first coordination sphere, which is better in case of chloro and nitro groups, it is possible to explain why Cl^- or NO_3^- complexes have greater activity than CH_3COO^- complexes (Panja et al., 2018). The comparable efficacy may also be elucidated based on the steric impact brought on by the CH_3COO^- group's bulkiness when compared to Cl^- or NO_3^- .

4. Conclusion

H_2TNBS and H_2INBS azo dye ligands which synthesized by coupling of sulfathiazole and sulfafurazole diazonium salts and 2-hydroxy-1-naphthaldehyde were obtained and identified applying spectral and analytical ways. Both ligands were used for synthesizing Cu(II) chelates through their reaction with copper salts of different anions ($\text{CuCl}_2 \cdot 2\text{H}_2\text{O}$, $\text{Cu}(\text{CH}_3\text{COO})_2 \cdot \text{H}_2\text{O}$ and $\text{Cu}(\text{NO}_3)_2$). The structures of the obtained Cu(II) complexes have been assured to be all square planar in geometry with 1:1 (M:L) composition for H_2INBS chelates and 2:1 (M:L) composition for H_2TNBS chelates. IR. Morphology of the synthesized compounds have been investigated using TEM technique which joint with the results of X-ray powder diffraction spectroscopy confirmed the precipitation of both ligands and their complexes in the nanometric scale. The compounds under interest have been tested for their activity against different bacterial and fungal strains showing, in most cases, enhancement of activity upon chelation. The antitumor activity of Cu(II) chelates and their ligands has been also examined against the cell lines A-549 cells (human Lung cancer cell line) and Panc-1 (Pancreatic carcinoma); standard drug vinblastin has been used for comparison. The compounds showed the order of activity to be $\text{H}_2\text{TNBS} < \text{H}_2\text{INBS} < \mathbf{6} < \mathbf{4} < \mathbf{5} < \mathbf{1} < \mathbf{3} < \mathbf{2}$ for A-549 cells and $\text{H}_2\text{TNBS} < \text{H}_2\text{INBS} < \mathbf{6} < \mathbf{4} < \mathbf{5} < \mathbf{1} < \mathbf{3} < \mathbf{2}$ for Panc-1 cells. Additionally, the synthesized complexes were estimated for their effectiveness as catalysts for oxidative coupling of 2-aminophenol to 2-

aminophenoxazine-3-one. The examined extremely high activity for the chloro complex **4** and nitro complex **6** with TOF numbers of 390.48 and 467.01 h^{-1} , respectively. The rest of compounds afforded TOF numbers ranging between 4.34 and 60.8 h^{-1} .

Declaration of Competing Interest

The authors declare that they have no known competing financial interests or personal relationships that could have appeared to influence the work reported in this paper.

Acknowledgements

The authors would like to thank the Deanship of Scientific Research at Umm Al-Qura University for supporting this work by Grant Code: (22UQU4281810DSR01).

Appendix A. Supplementary data

Supplementary data to this article can be found online at <https://doi.org/10.1016/j.arabj.2023.104916>.

References

- Ali, A., Chiang, Y.W., Santos, R.M., 2022. X-Ray Diffraction Techniques for Mineral Characterization: A Review for Engineers of the Fundamentals. Applications, and Research Directions, *Minerals*. 12, 205.
- Althagafi, I., Elghalban, M.G., El Metwaly, N.M., 2019. Novel Synthesized Benzenesulfonamide Nanosized Complexes; Spectral Characterization, Molecular Docking, Molecular Modeling and Analytical Application. *J. Inorg. Organomet. Polym. Mater.* 29, 876–892. <https://doi.org/10.1007/s10904-018-01062-3>.
- Awad, I.M.A., Osman, A.H., Aly, A.A.M. 2010. Heterocyclo-Substituted Sulfa Drugs : Part XII . Mercapto-S-Azo-Benzothiazol Dyes and Their Metal Complexes, Taylor & Francis Inc. 37–41.
- Benkhaya, S., M'rabet, S., El Harfi, A., 2020. Classifications, properties, recent synthesis and applications of azo dyes. *Heliyon* 6, e03271.
- Bentley, R., 2009. Different roads to discovery; Prontosil (hence sulfa drugs) and penicillin (hence β -lactams). *J. Ind. Microbiol. Biotechnol.* 36, 775–786.
- Cadranel, A., Oviedo, P.S., Pieslinger, G.E., Yamazaki, S., Kleiman, V.D., Baraldo, L.M., Guldi, D.M., 2017. Trapping intermediate

- MLCT states in low-symmetry Ru(bpy) complexes. *Chem. Sci.* 8, 17434–18142.
- A El-Ghamry, H., Takroni, K. M., AL-Rashidi, D. O., Alfear, E. S., Alsaedi, R. A. 2022. Design, spectral, thermal decomposition, antimicrobial, docking simulation and DNA binding tendency of sulfisoxazole azo dye derivative and its metal chelates with Mn^{2+} , Fe^{2+} , Co^{2+} , Ni^{2+} , Cu^{2+} , Zn^{2+} and Cd^{2+} , *Applied Organometallic Chemistry*, 36, e6813.
- Fawzy, A., Farghaly, T.A., El-Ghamry, H.A., Bawazeer, T.M., 2020. Investigation of the inhibition efficiencies of novel synthesized cobalt complexes of 1,3,4-thiadiazolethiosemicarbazone derivatives for the acidic corrosion of carbon steel. *J. Mol. Struct.* 1203, 127447.
- Feng, G., Zou, W., Zhong, Y., 2022. Sulfonamides repress cell division in the root apical meristem by inhibiting folates synthesis. *J. Hazard. Mater. Adv.* 5, 100045.
- Gaber, M., Khedr, A.M., Elsharkawy, M., 2017. Characterization and thermal studies of nano- synthesized Mn(II), Co(II), Ni(II) and Cu (II) complexes with adipohydrazone ligand as new promising antimicrobial and antitumor agents. *Appl. Organomet. Chem.* 31.
- Gaber, M., Khedr, A.M., Mansour, M.A., Elsharkawy, M., 2018. Nano-synthesis, characterization, modeling and molecular docking analysis of Mn (II), Co (II), Cr (III) and Cu (II) complexes with azo pyrazolone ligand as new favorable antimicrobial and antitumor agents. *Appl. Organomet. Chem.* 32 (12), e4606.
- Gaffer, H.E., 2019. Antimicrobial sulphonamide azo dyes. *Color. Technol.* 135, 484–500.
- Gamberi, T., Hanif, M., 2022. Metal-Based Complexes in Cancer Treatment. *Biomedicines.* 10. 6–8 2573.
- Gasque, L., Mendieta, A., Ferrer-Sueta, G. 2020. Comment on “mixed azido/phenoxido bridged trinuclear Cu(II) complexes of Mannich bases: Synthesis, structures, magnetic properties and catalytic oxidase activities”: *Dalton Trans.*, 2018, 47, 9385–9399 and “tri-And hexa-nuclear NiII-MnII complexes of a N2O2 donor unsymmetrical ligand: Synthesis, structures, magnetic properties and catalytic oxidase activities”, *Dalton Trans.*, 47 (2018) 13957–13971, *Dalt. Trans.* 49 (2020) 3365–3368.
- Gawrońska, M., Kowalik, M., Duch, J., Kazimierczuk, K., Makowski, M., 2022. Sulfonamides with hydroxyphenyl moiety: Synthesis, structure, physicochemical properties, and ability to form complexes with Rh(III) ion. *Polyhedron.* 221, 115865.
- Geary, W.J., 1971. The use of conductivity measurements in organic solvents for the characterisation of coordination compounds. *Coord. Chem. Rev.* 7, 81–122.
- Gladys, G., Claudia, G., Marcela, L., 2003. The effect of pH and triethanolamine on sulfisoxazole complexation with hydroxypropyl- β -cyclodextrin. *Eur. J. Pharm. Sci.* 20, 285–293.
- Gokcen, T., Gulcin, I., Ozturk, T., Goren, A.C., 2016. A class of sulfonamides as carbonic anhydrase I and II inhibitors. *J. Enzyme Inhib. Med. Chem.* 31, 180–188.
- Guo, Z., Xu, Y., Peng, Y., Rashid, Haroon ur, Quan, W., Xie, P., Wu, L., Jiang, J., Wang, L., Liu, X., 2019. Design, synthesis and evaluation of novel (S)-tryptamine derivatives containing an allyl group and an aryl sulfonamide unit as anticancer agents. *Bioorganic Med. Chem. Lett.* 29 (9), 1133–1137.
- Iakovidis, I., Delimaris, I., Piperakis, S.M., 2011. Copper and Its Complexes in Medicine: A Biochemical Approach. *Mol. Biol. Int.* 2011, 1–13.
- Islam, M., Mondal, P., Mondal, S., Mukherjee, S., Roy, A.S., Mubarak, M., Paul, M., 2010. Use of a New Polymer Anchored Cu(II) Azo Complex Catalyst for the Efficient Liquid Phase Oxidation Reactions. *J. Inorg. Organomet. Polym.* 20, 87–96.
- Jahangirian, H., Haron, M.D.J., Shah, M.H., Rafiee-Moghaddam, E. R., Afsah-Hejri, L., Abdollahi, Y., Rezayi, M., Vafaei, N., 2013. Well Diffusion Method for Evaluation of Antibacterial Activity of copper phenyl fatty hydroxamate synthesized from canola and palm kernel oils. *J. Nanomater. Biostructures.* 8, 1263–1270.
- Kamal, A., Naseer, M., Khan, A., Reddy, K.S., Rohini, K., Sastry, G. N., Sateesh, B., Sridhar, B., 2007. Synthesis, structure analysis, and antibacterial activity of some novel 10-substituted 2-(4-piperidyl/phenyl)-5,5-dioxo[1,2,4]triazolo[1,5-b][1,2,4]benzothiadiazine derivatives, *Bioorganic Med. Chem. Lett.* 17, 5400–5405.
- Kanaani, A., Ajloo, D., Grivani, G., Ghavami, A., Vakili, M., 2016. Tautomeric stability, molecular structure, NBO, electronic and NMR analyses of salicylideneimino-ethylimino-pentan-2-one. *J. Mol. Struct.* 1112, 87–96.
- Khan, S., Muhammad, M., Al-Saidi, H.M., Hassanian, A.A., Alharbi, W., Alharbi, K.H., 2022. Synthesis, characterization and applications of schiff base chemosensor for determination of Cu^{2+} ions. *J. Saudi Chem. Soc.* 26, 101503.
- Khatab, T.A., Haggag, K.M., Elnagdi, M.H., Abdelrahman, A.A., Abdelmoez Aly, S., 2016. Microwave-Assisted Synthesis of Arylamino-pyrazoles as Disperse Dyes for Textile Printing, *Zeitschrift Fur Anorg. Und Allg. Chemie.* 642, 766–772.
- Khedr, A.M., El-Ghamry, H., Kassem, M.A., Saad, F.A., El-Guesmi, N., 2019. Novel series of nanosized mono- and homobi-nuclear metal complexes of sulfathiazole azo dye ligand: Synthesis, characterization, DNA-binding affinity, and anticancer activity. *Inorg. Chem. Commun.* 108, 107496.
- Khedr, A.M., El-Ghamry, H.A., El-Sayed, Y.S., 2022. Nano-synthesis, solid state structural characterization, antimicrobial and anticancer assessment of new sulfafurazole azo dye-based metal complexes for further pharmacological applications. *Appl. Organomet. Chem.* 36, e6548.
- Khedr, A.M., Gouda, A.A., El-Ghamry, H.A., 2022. Nano-synthesis approach, elaborated spectral, biological activity and in silico assessment of novel nano-metal complexes based on sulfamerazine azo dye. *J. Mol. Liq.* 352, 118737.
- Kumasaka, K., Kojima, T., Doi, K., Satoh, S., 2003. Analysis of the oral hypoglycemic agent, glibenclamide, in a health food. *Yakugaku Zasshi.* 123, 1049–1054.
- Lee, S., Roesel, D., Roke, S., 2021. Imaging Cu^{2+} binding to charged phospholipid membranes by high-throughput second harmonic wide-field microscopy. *Chem. Phys.* 155, 184704.
- Li, J.M., Jin, X., 2009. Synthesis, crystal structure, and magnetism of a binuclear Cu(II) complex with a single end-to-end bridged azido ligand. *J. Coord. Chem.* 62, 2610–2615.
- Mandal, A., Sarkar, A., Adhikary, A., Samanta, D., Das, D., 2020. Structure and Synthesis of Copper Based Schiff base and Reduced Schiff base Complex: A Combined Experimental and Theoretical Investigation of Biomimetic Catalytic Activity. *Dalton Trans.* 49, 15461–15472.
- Mizdal, C.R., Stefanello, S.T., da Costa Flores, V., Agertt, V.A., Benez, P.C., Rossi, G.G., da Silva, T.C., Antunes Soares, F.A., de Lourenço Marques, L., de Campos, M.M.A., 2018. The antibacterial and anti-biofilm activity of gold-complexed sulfonamides against methicillin-resistant *Staphylococcus aureus*. *Microb. Pathog.* 123, 440–448.
- Mohamed, M.T., Mabrouk, E.M., 2006. Voltammetric, potentiality and thermodynamic studies of some rhodanine sulfa drugs azo compounds in aqueous solutions 3, 155–164.
- Mosmann, T., 1983. Rapid colorimetric assay for cellular growth and survival: application to proliferation and cytotoxicity assays. *J. Immunol. Methods* 65, 55–63.
- Olar, R., Badea, M., Ilis, M., Negreanu-Pirjol, T., Calinescu, M., 2013. Studies on thermal behavior of some antibacterial copper (II) complex compounds with a dibiguanide derivative ligand. *J. Therm. Anal. Calorim.* 111, 1189–1195.
- Oloyede, H.O., Woods, J.A.O., Görls, H., Plass, W., Eseola, A.O., 2019. The necessity of free and uncrowded coordination environments in biomimetic complex models: oxidative coupling by mixed-ligand cobalt(II) complexes of diazene-disulfonamide. *New J. Chem.* 43, 18322–18330.
- Panja, A., Jana, N.C., Brandão, P., 2018. Influence of anions and solvents on distinct coordination chemistry of cobalt and effect of coordination spheres on the biomimetic oxidation of o-aminophenols. *Mol. Catal.* 449, 49–61.

- Podder, N., Mandal, S., 2020. Aerobic oxidation of 2-aminophenol catalysed by a series of mononuclear copper(II) complexes: phenoxazinone synthase-like activity and mechanistic study. *New J. Chem.* 44, 12793–12805.
- Riyadh, S.M., Gomha, S.M., Mahmmoud, E.A., Elaasser, M.M., 2015. ChemInform Abstract: Synthesis and Anticancer Activities of Thiazoles, 1,3-Thiazines, and Thiazolidine Using Chitosan-Grafted-Poly(vinylpyridine) as Basic Catalyst. *ChemInform.* 46.
- Saad, F.A., Elghalban, M.G., El-Metwaly, N.M., El-Ghamry, H., Khedr, A.M., 2017. Density functional theory/B3LYP study of nanometric 4-(2,4-dihydroxy-5-formylphen-1-ylazo)-N-(4-methylpyrimidin-2-yl)benzenesulfonamide complexes: Quantitative structure–activity relationship, docking, spectral and biological investigations. *Appl. Organomet. Chem.* 31, 1–15.
- Saad, F.A., Al-Fahemi, J.H., El-Ghamry, H., Khedr, A.M., Elghalban, M.G., El-Metwaly, N.M., 2018. Elaborated spectral, modeling, QSAR, docking, thermal, antimicrobial and anticancer activity studies for new nanosized metal ion complexes derived from sulfamerazine azodye. *J. Therm. Anal. Calorim.* 131, 1249–1267.
- Saad, F.A., El-Ghamry, H.A., Kassem, M.A., Khedr, A.M., 2019. Nano-synthesis, Biological Efficiency and DNA Binding Affinity of New Homo-binuclear Metal Complexes with Sulfa Azo Dye Based Ligand for Further Pharmaceutical Applications. *J. Inorg. Organomet. Polym. Mater.* 29, 1337–1348.
- Saad, F.A., El-Ghamry, H.A., Kassem, M.A., 2019. Synthesis, structural characterization and DNA binding affinity of new bioactive nano-sized transition metal complexes with sulfathiazole azo dye for therapeutic applications. *Appl. Organomet. Chem.* 33, 1–14.
- Samper, K.G., Marker, S.C., Bayón, P., MacMillan, S.N., Keresztes, I., Palacios, Ó., Wilso, J.J., 2017. Anticancer activity of hydroxy- and sulfonamide-azobenzene platinum(II) complexes in cisplatin-resistant ovarian cancer cells. *J Inorg Biochem.* 174, 102–110.
- Sanad, M.M.S., Elsharif, S.S., Eraky, M.S., Abdel-Monem, Y.K., 2022. Hetero-valent cations- doped zinc stannate nanoparticles for optoelectronic and dielectric applications. *Mater. Chem. Phys.* 291, 126700.
- Sarkar, N., Das, M., Chattopadhyay, S., 2017. Two new manganese (III) complexes with salicylaldehyde Schiff bases: Synthesis, structure, self-assembly and phenoxazinone synthase mimicking activity. *Inorganica Chim. Acta.* 457, 19–28.
- Scozzafava, A., Owa, T., Mastrolorenzo, A., Supuran, C.T., 2003. Anticancer and Antiviral Sulfonamides. *Curr. Med. Chem.* 10, 925–953.
- Singh, B.K., Jetley, U.K., Sharma, R.K., Garg, B.S., 2007. Synthesis, characterization and biological activity of complexes of 2-hydroxy-3,5-dimethylacetophenoneoxime (HDMAOX) with copper(II), cobalt(II), nickel(II) and palladium(II), *Spectrochim. Acta – Part A Mol. Biomol. Spectrosc.* 68, 63–73.
- Sohtun, W.P., Muthuramalingam, S., Sankaralingam, M., Velusamy, M., Mayilmurugan, R., 2021. Copper(II) complexes of tripodal ligand scaffold (N_3O) as functional models for phenoxazinone synthase. *J. Inorg. Biochem.* 216, 111313.
- Supuran, C.T., 2008. Diuretics: From Classical Carbonic Anhydrase Inhibitors to Novel Applications of the Sulfonamides. *Curr. Pharm. Des.* 14, 641–648.
- Takroni, K.M., Farghaly, T.A., Harras, M.F., El-Ghamry, H.A., 2020. Synthesis, structure elucidation, DNA binding and molecular docking studies of novel copper (II) complexes of two 1,3,4-thiadiazolethiosemicarbazone derivatives. *Appl. Organomet. Chem.* 34, 1–16 e5860.
- Uhlemann, T., Seidel, S., Müller, C.W., 2018. Site-specific binding of a water molecule to the sulfa drugs sulfamethoxazole and sulfisoxazole: a laser-desorption isomer-specific UV and IR study. *Phys. Chem. Chem. Phys.* 20, 6891–6904.
- Uysal, Ş., Kuruşunlu, A.N., 2011. The Synthesis and Characterization of Star Shaped Metal Complexes of Triazine Cored Schiff Bases: Their Thermal Decompositions and Magnetic Moment Values. *J. Inorg. Organomet. Polym. Mater.* 21, 291–296.
- Wan, Y., Fang, G., Chen, H., Deng, X., Tang, Z., 2021. Sulfonamide derivatives as potential anti-cancer agents and their SARs elucidation. *Eur. J. Med. Chem.* 226, 113837.
- Weber, A., Casini, A., Heine, A., Kuhn, D., Supuran, C.T., Scozzafava, A., Klebe, G., 2004. Unexpected Nanomolar Inhibition of Carbonic Anhydrase by COX-2-Selective Celecoxib: New Pharmacological Opportunities Due to Related Binding Site Recognition. *J. Med. Chem.* 47, 550–557.
- Xu, F., Min, F., Wang, J., Luo, Y., Huang, S., Chen, M., Wu, R., Zhang, Y., 2020. Development and evaluation of a Luminex xTAG assay for sulfonamide resistance genes in *Escherichia coli* and *Salmonella* isolates. *Mol. Cell. Probes.* 49, 101476.
- Yarkandi, N.H., El-Ghamry, H.A., Gaber, M., 2017. Synthesis, spectroscopic and DNA binding ability of Co^{II} , Ni^{II} , Cu^{II} and Zn^{II} complexes of Schiff base ligand (E)-1-(((1H-benzo[d]imidazol-2-yl)methylimino)methyl)naphthalen-2-ol. X-ray crystal structure determination of cobalt (II) complex. *Mater. Sci. Eng.* 75, 1059–1067.